Sussex Research Online

A state-dependent damping method to reduce collision force and its variability

Article (Published Version)

Hamid, Elham, Herzig, Nicolas, Abad Guaman, Sara Adela and Nanayakkara, Thrishantha (2021) A state-dependent damping method to reduce collision force and its variability. IEEE Robotics and Automation Letters. ISSN 2377-3766

This version is available from Sussex Research Online: http://sro.sussex.ac.uk/id/eprint/97570/

This document is made available in accordance with publisher policies and may differ from the published version or from the version of record. If you wish to cite this item you are advised to consult the publisher's version. Please see the URL above for details on accessing the published version.

Copyright and reuse:
Sussex Research Online is a digital repository of the research output of the University.

Copyright and all moral rights to the version of the paper presented here belong to the individual author(s) and/or other copyright owners. To the extent reasonable and practicable, the material made available in SRO has been checked for eligibility before being made available.

Copies of full text items generally can be reproduced, displayed or performed and given to third parties in any format or medium for personal research or study, educational, or not-for-profit purposes without prior permission or charge, provided that the authors, title and full bibliographic details are credited, a hyperlink and/or URL is given for the original metadata page and the content is not changed in any way.

http://sro.sussex.ac.uk

This article has been accepted for publication in a future issue of this journal, but has not been fully edited. Content may change prior to final publication. Citation information: DOI 10.1109/LRA.2021.3062307, IEEE Robotics and Automation Letters

A State-Dependent Damping Method to Reduce Collision Force and Its Variability

E. Hamid[1], N. Herzig[2], S-A. Abad[3], and T. Nanayakkara[4], *Senior Member, IEEE,*

***Abstract*—This paper investigates the effect of biologically inspired angle-dependent damping profile in a robotic joint primarily on the magnitude and the variability of the peak collision force. Joints such as the knee that experience collision forces are known to have an angle-dependent damping profile. In this paper, we have quantified and compared three damping profiles. Our numerical and experimental results show that the proposed hyperbolic angle-dependent damping profile can minimize both the magnitude and the variability of the peak collision force (average magnitude and variability reduction of $\approx 26\%$ and $\approx 47\%$ compared to the peak constant damping profile). Very often, the variability of the force across the collision between the robot and the environment cause uncertainty about the state variables of the robotic joint. We show that by increasing the slope of the proposed hyperbolic angle-dependent damping profile we can also reduce the variability and the magnitude of post-collision peak displacement and peak velocity compared to those of constant damping profile. This was achieved while reducing the root mean square of power consumed by the robotic joint.**

***Index Terms*—Actuation and Joint Mechanisms, Compliance and Impedance Control**

I. Introduction

MINIMISING collision force and its variability is important for many robotic applications such as legged locomotion and collaborative robots (cobots). There are several methods for collision avoidance [1], [2]. However, there are robotic applications where contact is part of the task, such as legged locomotion, object passing, physical examination, etc. In such tasks, predictability depends on both the collision force and its variability. It is believed that for most animals, one of the top priorities is to minimise the peak collision force to reduce the risk of injury and permanent joint damages [3]. Furthermore, it is known that the knee joint not only manages to decrease the magnitude but also the variability of the force as well as the motion variability doing a similar task at a similar ground condition [4]. However, it is a complex computational problem to adjust the internal impedance of a robotic joint to decrease the variability of one quantity without compromising that of another quantity [5].

The dynamics of systems that involve periodic impulsive collisions with the environment cause sudden jumps in the state-space, which varies at each step on the same terrain [6], [7]. Previous research on a simple passive dynamic walker known as the rimless wheel has revealed that the distribution of the coefficient of restitution and the coefficient of friction and their interactions play a significant role in the state variability [8]. Therefore, any solution that would reduce the variability of states upon collisions will help to reduce the chances of failure.

The complexity in robot-environment interaction that involves dynamics that are punctuated by collisions is a major challenge for closed-loop control systems. Several studies have investigated fast collision detection and reactive behaviour mechanisms [9]–[11] or different numerical methods of predicting the consequence of variability on the stability [12], [13] or search for impedance parameters that can reduce the variability [14]. However, in the studies mentioned above, intensive computational algorithms for real-time control were used.

Based on laws governing interaction dynamics, body in dynamic association with the environment should adjust its internal impedance to preserve a stable dynamic coupling with the environment [15]. The knee joint is an example that is vital for efficiency and stability of legged locomotion in human and animals [5], [16]. However, its variable impedance (stiffness, damping, and inertia) [17] and its computational role in walking remain to be understood.

In this paper, we focus on implementing a simple active impedance control method that can better emulate the morphological impedance profile of the knee joint to be implemented in any robotic joint and to provide efficient and stable behaviour. Indeed angle-dependent stiffness is also important, however studying the combined effect of angle-dependent stiffness and angle-dependent damping is beyond the scope of this paper. Furthermore, it is known that the damping profile can intrinsically stabilise the system [18]. This study focuses not only on the magnitude but also on the variability of the collision force, post-collision peak displacement and velocity. We propose a hyperbolic angle-dependent damping control framework that can be easily implemented in each motor of

Manuscript received: 10, 13, 2020; Revised 1, 10, 2021; Accepted 2, 6, 2021.

This paper was recommended for publication by Editor Clement Gosselin upon evaluation of the Associate Editor and Reviewers' comments. This work was supported in part by the Engineering and Physical Sciences Research Council (EPSRC) MOTION grant (EP/N03211X/2 and EP/N03208X/1), and EPSRC RoboPatient grant (EP/T00603X/1).

[1]Elham Hamid is with Centre for Robotics Research, Department of Informatics, King's College London, London WC2R 2LS, UK. elham.hamid@kcl.ac.uk

[2] Nicolas Herzig is with the School of Engineering and Informatics, University of Sussex, Brighton, BN1 9QT, UK. nh366@sussex.ac.uk

[3] Sara-Adela Abad is with the Department of Mechanical Engineering, UCL, London, WC1E 7JE, UK; and with the Institute for Applied Sustainability Research, Av. Granados E13-55 e Isla Marchena, No.44, Quito, 170503, Ecuador. s.abad-guaman@ucl.ac.uk

[4]Thrishantha Nanayakkara is with Dyson School of Design Engineering, Imperial College London, London SW7 2DB, UK. t.nanayakkara@imperial.ac.uk

Digital Object Identifier (DOI): see top of this page.

This work is licensed under a Creative Commons Attribution 4.0 License. For more information, see https://creativecommons.org/licenses/by/4.0/

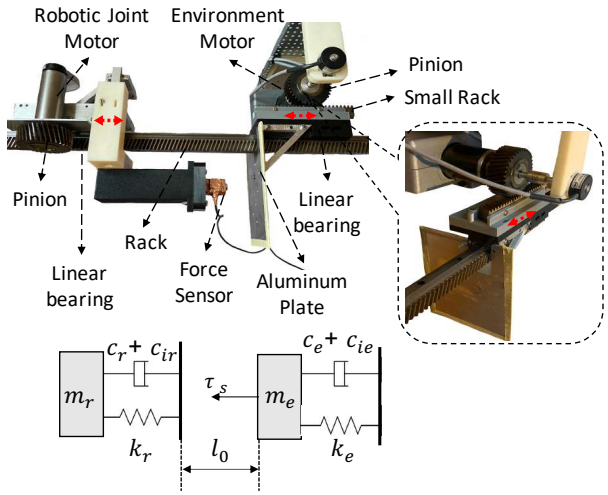

Fig. 1. Experimental setup: The force sensor measures the collision force at the point of contact between the robot and the aluminium plate representing the environment. To replicate the impact between a robot with the environment, the motor representing the environment was set to move the aluminum plate sinusoidally. The angle of rotation of the robotic joint motor, represents the robot joint angle.

a robot. We provide analytical and experimental validations of this generic method. The results show that it minimised both the variability and magnitude of the peak collision force as well as that of the post-collision peak velocity and peak displacement without complicated computations. Interestingly, this was achieved while minimising the root mean square of power. To isolate the effect of the hyperbolic angle-dependent damping profile on a robotic joint, we keep a constant proportional gain and conduct experiments in the horizontal plane to only study the normal force.

II. ANGLE-DEPENDENT DAMPING CONTROL

Zhang et al. [17] found out that the internal impedance of a human's knee joint is a nonlinear function of the joint angle. Furthermore, Morland et al. [19], showed that an angle-dependent damping control could provide better control in legged locomotion using a rimless wheel. However, a quantification of the angle-depended damping profile remains to be performed. In the contact phase of the feet with the environment, using the impedance control (controlling the stiffness, damping and inertia), the knee joint manages the impact during the strike, and it provides stability by absorbing and controlling the collision force [16]. By taking the viscosity values from [17] for a given constant torque value and plotting them against their joint angles, the damping profile of the knee joint (shown in Fig. 2) was obtained. During the strike, the damping profile can be approximated as a hyperbolic function because the knee joint angle varies in a small range between 10° and 25° on average [20]. Active impedance control for the knee joint is obtained by muscular control of co-contracting antagonistic muscle pairs which can control the joint torques in humans and animals [21]. There are two ways of taking inspiration from the knee joint, one is to design the cam profile of the knee, and the other is to incorporate its properties into

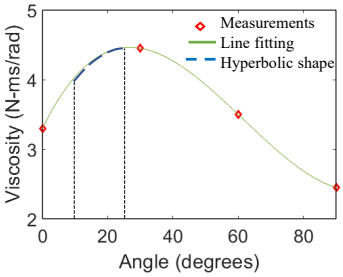

Fig. 2. The damping profile of the knee joint against the knee joint angle. This profile is based on the viscosity values and their corresponding joint angles, provided in [17], at a given constant torque value.

a controller. We do not intend to exactly mimic the biology of the knee joint, but we intend to take inspiration from its control over the impedance properties. We approximate the angle-dependent damping profile found by Zhang et al. [17] to a hyperbolic function of the joint angle ($c_h(\theta_r)$) given by:

$$c_h(\theta_r) = c_0 + (c_{max} - c_0)(1 - e^{-\eta|\theta_r|}) \quad (1)$$

where θ_r is the angle of the robotic joint. Zhang et al. [17] also showed that at the relaxed state and zero degree flexion, the knee joint damping coefficient is not zero. Saying that $c_0 = 0.2$ Ns/rad represents the minimum damping coefficient of a robotic joint. $c_{max} = 5$ Ns/rad refers to the maximum damping coefficient of the robotic joint. These parameters are set to be constants for both simulation and experiment. $(c_{max} - c_0)$ is to prevent the damping coefficient of the joint exceeding the minimum and maximum damping coefficients of the joint. $(1 - e^{-\eta|\theta_r|})$ provides hyperbolic shape of the damping. Where η is a scaling factor in the angle-dependent damping function determining its slope ($\eta \in [0, 0.5, 1, 1.5]$). In other words, increasing η rises the damping coefficient c_h. The values are chosen based on the limitation of the experimental setup. Furthermore, since the proposed function is angle-dependent, a periodic damping profile would be achieved for periodic angle variation.

III. EXPERIMENTAL SETUP

To represent the during collision phase and before and after collision phase of a robotic joint with the environment, we developed an experimental setup shown in Fig. 1. A PD controlled back-drivable MAXON motor (EC-max 40 mm, 120 W, brush-less, geared at $1:81$ gearing ratio, motor part number 283873) was used to provide active impedance control of the robotic joint as a function of its angle θ_r. This motor was attached to an 8 cm diameter pinion. The proportional ($K_p = 8$) gain was set to be constant, and the derivative (K_d) gain was controlled as a function of θ_r.

To represent the environment (any object that comes into contact with the robot), an aluminium plate attached to a small horizontal rack was set to be in contact with another 8 cm diameter pinion. The pinion was attached to another MAXON motor (EC 60 mm, 400 W, brush-less, part number 167131) with high PD gains ($K_p = 30000$ and $K_d = 3772$). Therefore, its position and velocity will not be affected when colliding

This article has been accepted for publication in a future issue of this journal, but has not been fully edited. Content may change prior to final publication. Citation information: DOI 10.1109/LRA.2021.3062307, IEEE Robotics and Automation Letters

with the robot. Each MAXON motor was connected to an EPOS $5/50$. The collision force was measured by a 50 N Load Cell attached to the 3D printed part connected to the motor representing the robotic joint.

This paper intends to show the effect of the hyperbolic angle-dependent damping profile on a robotic joint. Since the torque contributed by gravity also changes with the joint angle, for clarity, the gravity effect of the robot was removed. Furthermore, to only study the normal force at the point of contact, both motors were constrained to move horizontally.

IV. Analytical Model

In this work, the motor representing the environmental object follows a sinusoidal movement. As shown in the schematic design of the experimental setup (1), τ_s is the torque for the desired sinusoidal motion of the environmental object and is given by:

$$\tau_s = k_e\theta_e^* + (c_e + c_{ie})\dot{\theta}_e^* \tag{2}$$

where $k_e = 90$ N/rad, $c_e = 9$ Ns/rad, θ_e and $\theta_e^* = l_0 + A\sin(2\pi ft)$ are the constant stiffness, damping, and the actual and desired joint angle of the motor representing the environment. $l_0 = 4.7$ rad, $A = 4.97$ rad, $f = 1$ Hz, and t s are the initial distance of the environmental object from the robot, amplitude, frequency and time. $\dot{\theta}_e$ and $\dot{\theta}_e^*$ are the actual and desired velocity of the motor representing the environment. The aim of this research is to study the effect of a hyperbolic angle-dependent damping control of a robotic joint actuator on the collision force denoted F_c. Simulations were conducted for two phases of relative movement between the environmental object and the robot; before and after collision phase and during collision phase. The state space representation of the system is in the form of $\dot{\mathbf{x}} = A\mathbf{x} + B\tau_s$. The state vector is described by: $\mathbf{x} = \begin{bmatrix}\theta_r & \dot{\theta}_r & \theta_e & \dot{\theta}_e\end{bmatrix}^T$ and $B = [0\ 0\ 0\ 1/J_e]^T$. Where the A matrix that holds the physical system's information for either during collision phase or before and after collision phase.

A. During Collision Phase

The model represents an elastic collision, perpendicular to the plane of impact, with a spring and a damper in parallel acting between the two objects that come into contact (robot and environment). Two phases were considered: when the robot and the environmental object are independent, and when they are coupled during impact. The conservation of momentum is applied to the two objects during the transition from one phase to another. When the robotic joint comes into contact with the environmental object, the system's dynamics changes to a double-mass-spring-damper system. Then the equations of motion of the system at the contact phase can be used to find the collision force. The A matrix for during collision phase (A_c) is given by:

$$A_c = \begin{bmatrix} 0 & 1 & 0 & 0 \\ \frac{-k_r}{J_r} & \frac{-c_h(\theta_r)-c_{ir}}{J_r} & \frac{k_r}{J_r} & \frac{c_h(\theta_r)+c_{ir}}{J_r} \\ 0 & 0 & 0 & 1 \\ \frac{k_r}{J_e} & \frac{c_h(\theta_r)+c_{ir}}{J_e} & \frac{-k_r-k_e}{J_e} & \frac{-c_h(\theta_r)-c_{ir}-c_e-c_{ie}}{J_e} \end{bmatrix} \tag{3}$$

where θ_r and $\dot{\theta}_r$ are the angular displacement and velocity of the motor representing the robotic joint. Parameter J_e is defined as $J_e = I_{gm} + I_p + m_e r^2$. Where $I_{em} = 8.01e^{-5}$ kgm^2, $I_p = 6.4e^{-4}$ kgm^2 and $m_e = 12.4$ kg are moment of inertia of the motor representing the environment and the moment of inertia of the pinion, as well as the total mass that the motor representing the environment must move (the aluminium plate and the small rack attached to it). $r = 4$ cm refers to the radius of motor's pinion. Parameter J_r is defined as $J_r = I_{rm} + I_p + m_r r^2$. Where $I_{rm} = 1.01e^{-5}$ kgm^2 refers to the moment of inertia of the motor representing the robotic joint. The inertia of the link of the robot in contact with the environment is negligible in comparison to the inertia of the environment. The total mass of the robotic joint's motor has to move is $m_r = 8.2$ kg. As explained in section II, $c_h(\theta_r)$ represents the hyperbolic angle-dependent damping of the robotic joint controlled by (1). Parameter $k_r = 8$ N/rad, is the stiffness coefficient of the robotic joint motor. $c_{ir} = 0.8$ Ns/rad and $c_{ie} = 0.4$ Ns/rad are the coefficient of friction/damping of the robotic joint motor and the environmental object motor. The torque applied to the robot during the normal collision between the robot and the environment, $\tau_c(\theta_r)$ is given by:

$$\tau_c(\theta_r) = -\left(c_h(\theta_r) + c_{ir}\right)\left(\dot{\theta}_r - \dot{\theta}_e\right) - k_r(\theta_r - \theta_e) \tag{4}$$

where the collision force F_c applied to the robot at the point of contact is $F_c = \tau_c(\theta_r)/r$. Observing the torque coming from the PD controller of the robotic joint motor and angle of the robotic joint, we can compute the power P of the robotic joint regulating the impedance, $P = \tau_r(\theta_r)\dot{\theta}_r$. Where $\tau_r(\theta_r)$ is the torque coming from the PD controller of the robotic joint actuator given by:

$$\tau_r(\theta_r) = (c_h(\theta_r) + c_{ir})\dot{\theta}_r + k_r\theta_r \tag{5}$$

B. Before and After Collision Phase

For before and after the collision where there is no contact between the robot and the environmental object, the physical system's information matrix (A_i) is given by:

$$A_i = \begin{bmatrix} 0 & 1 & 0 & 0 \\ \frac{-k_r}{J_r} & \frac{-c_h(\theta_r)-c_{ir}}{J_r} & 0 & 0 \\ 0 & 0 & 0 & 1 \\ 0 & 0 & \frac{-k_e}{J_e} & \frac{-c_e-c_{ie}}{J_e} \end{bmatrix} \tag{6}$$

V. Coefficient of Variation Analysis

In robotic applications that involve dynamics that are punctuated by impulsive collisions with the environment, predictability and consequently stability depends on minimizing both the magnitude and variability of the peak collision force as well as the state variability (displacement and velocity). Therefore, In this research when comparing our proposed method with other two constant damping profiles, the summation of the coefficient of variation of the collision force Cv_F, angular peak velocity Cv_v and peak displacement Cv_d of the robotic joint should be calculated and compared.

$$Cv_F = \frac{\sigma F_c}{\mu F_c},\ Cv_v = \frac{\sigma\dot{\theta}_r}{\mu\dot{\theta}_r},\ Cv_d = \frac{\sigma\theta_r}{\mu\theta_r} \tag{7}$$

$$Cv_r = Cv_F + Cv_v + Cv_d \tag{8}$$

This work is licensed under a Creative Commons Attribution 4.0 License. For more information, see https://creativecommons.org/licenses/by/4.0/

This article has been accepted for publication in a future issue of this journal, but has not been fully edited. Content may change prior to final publication. Citation information: DOI 10.1109/LRA.2021.3062307, IEEE Robotics and Automation Letters

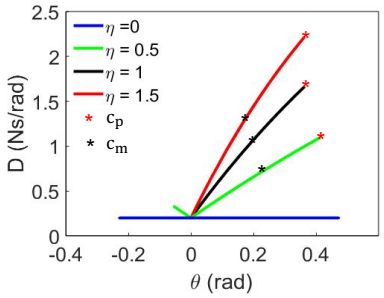

Fig. 3. An example of the damping profile found from the experiment on the hyperbolic angle-dependent damping function for different values of η. c_p is the maximum damping found at the maximum angle during the hyperbolic angle-dependent damping profile experiment and c_m is the damping value found at the middle of the hyperbolic angle-dependent damping profile.

where, σ and μ represent the standard deviation and the average of the state variables respectively. The aim is to find the damping profile that gives the minimum coefficient of variation of the robotic joint Cv_r.

$$\underset{\forall(C_r)\in\mathbb{R}}{\operatorname{argmin}}[Cv_r] \tag{9}$$

VI. Experimental procedure

Three sets of experiments were carried out. The first set of experiments was to test the effect of the proposed hyperbolic angle-dependent damping profile on the behaviour of a robotic joint. Then to evaluate the efficiency of our proposed function, the results from the first set of experiments were compared with two sets of different constant damping profiles (second and third set of experiments).

During the first set of experiments, the damping of the robotic joint PD controller was set to be the proposed hyperbolic angle-dependent damping ($c_r = c_h(\theta_r)$), found from (1). This was repeated for 10 trials, and the average of these 10 damping profiles was calculated. Fig. 3, presents a sample of a hyperbolic angle-dependent damping profile for all values of η. In order to see the effect of increasing damping coefficient on the magnitude and variability of the collision force as well as the state variables, this process was repeated for every value of $\eta \in [0, 0.5, 1, 1.5]$.

For the second experiment, the damping value reached at the maximum angle during each trial of the first experiment were found. After that, the average of the 10 maximum damping values c_p for each value of η was calculated and shown in Table I. Then for every value of η, the damping of the robotic joint PD controller was set to be these constant maximum damping values ($c_r = c_p$). These are the average of the applied damping values in the first set of experiments that control the displacement where the robotic joint was at its maximum joint angle. The results from the hyperbolic angle-dependent damping profile were compared with those for c_p. Therefore, for each value of η, the corresponding constant damping value of c_p was chosen and tested for 10 trials. With this experiment, we aim to compare the hyperbolic angle-dependent damping strategy with high constant damping strategy.

For the third experiment, rather than looking for the maximum damping values c_p, the damping values were chosen at the middle of the hyperbolic angle-dependent damping profile $c_m = \frac{c_p + c_0}{2}$. Therefore, for each value of η, the damping of the robotic joint PD controller was set to the constant damping values ($c_r = c_m$) shown in Table I. In addition, it can be observed that c_m and c_p increases as higher value of η is chosen (Table I). Basically, these three sets of experiments aimed to see the effect of our proposed angle-dependent damping function on the behaviour of a robotic joint in comparison to other constant damping. Note that, the environment-robotic joint strike was modelled as an inelastic collision.

TABLE I
Constant damping parameters for the experiment

η	$c_p(Ns/rad)$	$c_m(Ns/rad)$
0	0.2	0.2
0.5	1	0.6
1	1.6	0.9
1.5	2.18	1.19

VII. Results

A. Simulation results

The ODE113 function of MATLAB was used to solve the differential equations (6 and 3) derived previously. Then, the simulated results were plotted. Fig. 4(a) presents the simulation results for the peak collision force. It can be observed that by implementing our proposed hyperbolic angle-dependent damping profile c_h no matter what the value of η the peak collision force will stay constant around its minimum value. However, for the other two constant damping profiles (c_p and c_m) not only the peak collision force values were higher but they had a rising trend when increasing the value of η.

The post-collision peak velocity and displacement are shown in Fig. 4(b) and (c) respectively. It can be observed that for all three damping profiles, both the peak velocity and peak displacement decrease as the value of η increase. However, c_m shows higher peak velocity and displacement than our proposed damping profile c_h and peak constant damping profile c_p. Another factor to compare the performance of our proposed damping profile c_h with the other two constant damping profiles c_p and c_m was to calculate the root mean square of the power that was consumed to control the robotic joint. Fig. 4(d), shows that the proposed hyperbolic angle-dependent c_h provides lower root mean square of the power and c_p the highest. Table II presents the percentage of reduction when comparing the proposed hyperbolic angle-dependent damping profile c_h with the medium constant damping profile c_m ($\alpha = \frac{c_h - c_m}{c_m}\%$); as well as comparing the proposed hyperbolic angle-dependent damping profile c_h with the peak constant damping profile c_p ($\beta = \frac{c_h - c_p}{c_p}\%$).

B. Experimental results

Fig. 5 presents an example of the raw collision force data as well as the relative angular velocity between the robotic

This work is licensed under a Creative Commons Attribution 4.0 License. For more information, see https://creativecommons.org/licenses/by/4.0/

This article has been accepted for publication in a future issue of this journal, but has not been fully edited. Content may change prior to final publication. Citation information: DOI 10.1109/LRA.2021.3062307, IEEE Robotics and Automation Letters

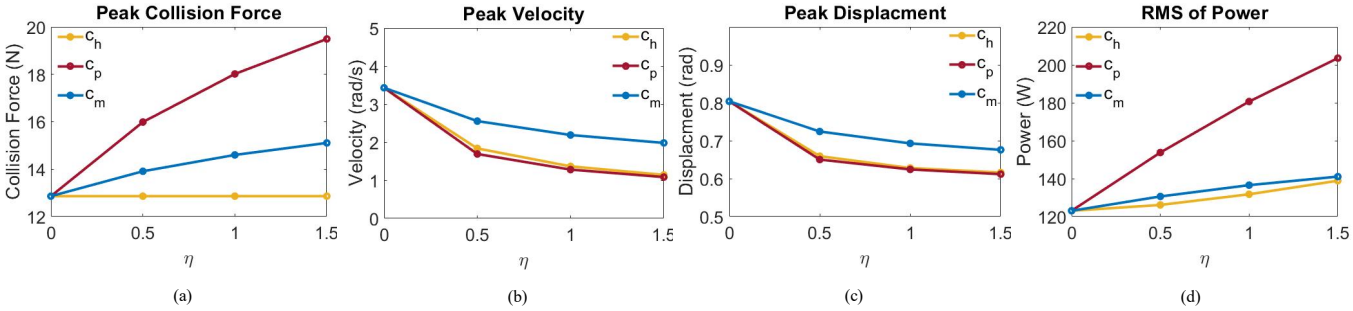

Fig. 4. Simulation results: (a) The peak collision force (b) the post-collision peak displacement, (c) the post-collision peak velocity, and (d) the root mean square of power for all three types of damping (c_h refers to our proposed hyperbolic angle-dependent damping profile, c_p and c_m refer to the maximum and medium constant damping profiles found from the first set of experiments) for every value of η. Which η represent the slope of the damping profile.

TABLE II
SIMULATION RESULTS: THE ANGLE-DEPENDENT DAMPING PROFILE VERSUS CONSTANT DAMPING PROFILES. THE NEGATIVE AND POSITIVE SIGNS REPRESENT THE REDUCTION AND INCREASE OF THE PARAMETERS RESPECTIVELY.

	Magnitude of Peak Collision Force		Magnitude of Peak Velocity		Magnitude of Peak Displacement		RMS of Power	
η	$\alpha\%$	$\beta\%$	$\alpha\%$	$\beta\%$	$\alpha\%$	$\beta\%$	$\alpha\%$	$\beta\%$
0.5	-41.984	-58.819	-23.974	1.706	-5.466	-1.330	-7.150	-28.265
1	-55.961	-71.291	-28.165	3.201	-0.622	0.826	-7.475	-35.987
1.5	-62.609	-76.466	-33.773	1.094	-3.028	-0.652	-2.878	-36.754

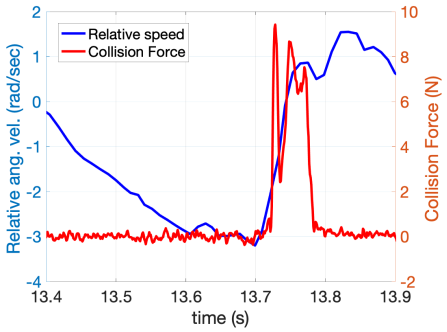

Fig. 5. An example of the force sensor reading for c_h at $\eta = 0$ and the corresponding relative angular velocity between the two actuators.

joint actuator and the environmental actuator. As it can be observed, the first peak of collision force causes a rise in the relative angular velocity due to the compliance of the robot actuator. This is followed by force and velocity oscillations due to the PD controllers of both actuators involved in the collision. As seen in Fig. 6(a), the proposed hyperbolic angle-dependent damping profile c_h resulted in the smallest average peak collision forces across all values of η. In addition, it was found that increasing the damping coefficient by increasing the values of η will not affect the peak collision force. Indeed, the peak collision forces were found to be similar $\approx$ 11 N. On the other hand, average peak collision force increased significantly for c_m and c_p, $\approx$ 14 N and $\approx$ 16 N respectively, compared to that for c_h. According to experimental results in Fig. 6(b) and (c), the peak displacement and post-collision peak velocity are decreasing for all three damping profiles (c_h, c_m and c_p) when the value of η increases. The average peak displacement and peak velocity for c_m were higher than the other two damping profiles. Interestingly, experiments show approximately equal average peak displacement for both c_h and c_p. The experimental results in Fig. 6(d) shows the root mean square of the power that was consumed by the robotic joint implementing different damping profiles. The root mean square of the power consumption for our proposed damping profile c_h was smaller than other constant damping profiles c_m and c_h. It can also be seen that the root mean square of the power consumption for both c_m and c_h are approximately equal at $\eta = 1$.

Fig. 7 presents the variation of peak collision force, post-collision peak velocity, as well as the peak displacement. The variability was measured by calculating the standard deviation of the values. Fig. 7(a) shows the variation of peak collision force. The experimental results for the proposed damping profile c_h, for all values of η, showed a higher negative trend on the variability. However, a gradual rise was mainly seen for c_m and c_p, except for c_m at $\eta = 1$. Fig. 7(b) presents the variability of the post-collision peak velocity. It can be observed that for every value of η, c_h provides a smaller variability of the post-collision peak velocity compared to c_m and c_p. Fig. 7(c) presents the variability of the peak displacement for each value of η and all three damping profiles. It can be observed that the lowest (0.012 for 3 significant decimal places) and highest variability (0.043) belong to the proposed damping profile c_h and the peak constant damping profile c_p respectively. In general, the standard deviation of the peak displacement is lower for our proposed damping profile c_h. Table III presents the percentage of reduction of

This work is licensed under a Creative Commons Attribution 4.0 License. For more information, see https://creativecommons.org/licenses/by/4.0/

This article has been accepted for publication in a future issue of this journal, but has not been fully edited. Content may change prior to final publication. Citation information: DOI 10.1109/LRA.2021.3062307, IEEE Robotics and Automation Letters

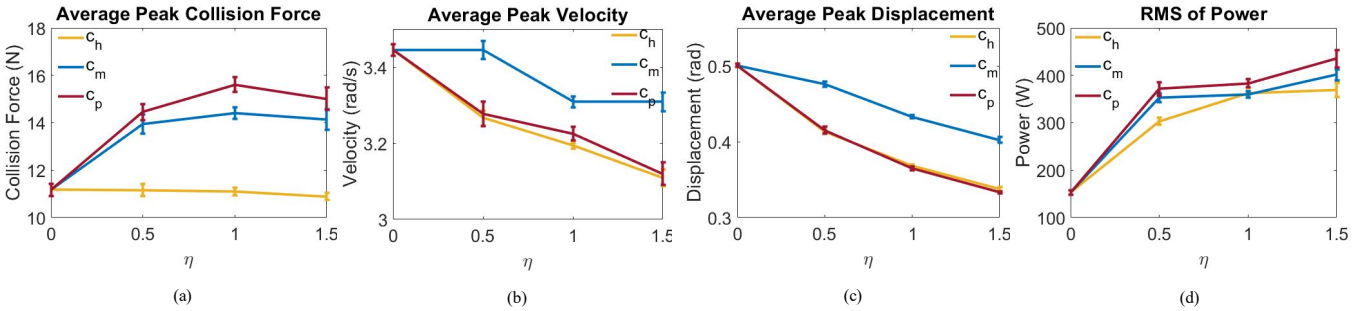

Fig. 6. Experimental results: (a) The average peak collision force (b) the average post-collision peak displacement, (c) the average post-collision peak velocity, and (d) the root mean square of power for all three types of damping (c_h, c_p and c_m) for every value of η. Which η represent the slope of the damping profile. The solid vertical lines indicate the error bar across the 10 trials for every value of η.

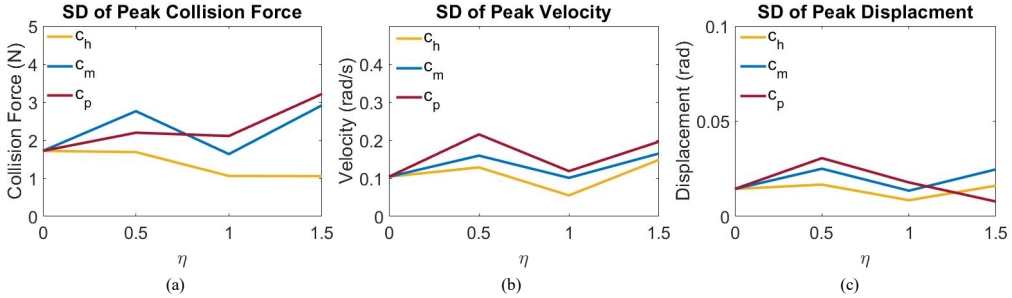

Fig. 7. Experimental results: The standard deviation of (a) the peak collision force, (b) the post-collision peak velocity, and (c) the post-collision peak displacement for all three types of damping (c_h, c_p and c_m) for every value of η which represent the slope of the damping profile.

TABLE III
EXPERIMENTAL RESULTS: THE ANGLE-DEPENDENT DAMPING PROFILE VERSUS CONSTANT DAMPING PROFILES.

	Magnitude of Peak Collision Force		Variability of Peak Collision Force		Magnitude of Peak Displacement		Variability of Peak Displacement		Magnitude of Peak Velocity		Variability of Peak Velocity		RMS of Power	
η	$\alpha\%$	$\beta\%$	$\alpha\%$	$\beta\%$	$\alpha\%$	$\beta\%$	$\alpha\%$	$\beta\%$	$\alpha\%$	$\beta\%$	$\alpha\%$	$\beta\%$	$\alpha\%$	$\beta\%$
0.5	-19.942	-22.768	-38.907	-23.202	13.083	-0.361	-34.002	-46.057	-5.167	-0.319	-19.360	-40.250	-14.273	-18.563
1	-23.092	-28.955	-35.085	-49.715	-14.899	0.945	-37.947	-52.440	-3.481	-0.974	-45.420	-53.591	0.779	-5.555
1.5	-22.984	-27.448	-63.776	-67.122	-16.064	1.395	-35.704	64.603	-6.012	-0.335	-10.109	-24.311	-7.953	-15.165

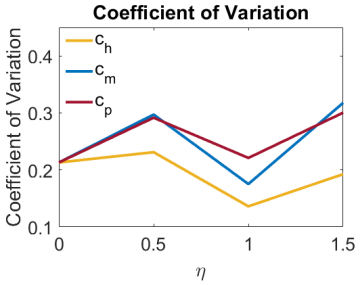

Fig. 8. Experimental results: The coefficient of variation of the robotic joint Cv_r for all three types of damping (c_h, c_p and c_m) and for every value of η.

magnitude and variability comparing the proposed hyperbolic angle-dependent damping profile c_h with the medium constant damping profile c_m ($\alpha\%$); as well as comparing the proposed hyperbolic angle-dependent damping profile c_h with the peak constant damping profile c_p ($\beta\%$). Fig. 8 compare the coefficient of variation of the robotic joint Cv_r for all three damping profiles. It can be observed that our proposed hyperbolic angle-dependent damping profile c_h provides the lowest Coefficient of variation in comparison to the other two constant damping profiles. Table IV present the percentage of reduction of the coefficient of variation of the robotic joint calculated for all three damping profiles.

VIII. DISCUSSION

Two factors are vital for systems that involve punctuated dynamics due to collisions; decreasing the magnitude of the peak collision forces and their variability [7], [8]. Furthermore, decreasing the variability of the peak collision force increases predictability and consequently, the stability of the robotic joint.

In this work, we proposed a biologically inspired hyperbolic angle-dependent damping profile that can be implemented in any robotic joint using a pure mechanical design, impedance control in a servo motor, or a mixed of the two. It was found that the proposed hyperbolic damping profile can significantly

This work is licensed under a Creative Commons Attribution 4.0 License. For more information, see https://creativecommons.org/licenses/by/4.0/

This article has been accepted for publication in a future issue of this journal, but has not been fully edited. Content may change prior to final publication. Citation information: DOI 10.1109/LRA.2021.3062307, IEEE Robotics and Automation Letters

reduce both the magnitude and the variability of the peak collision force. It is interesting to note that the collision force stayed around its minimum value irrespective of the value of η, the value of the damping coefficient (Fig. 4(a) and Fig. 6(a)). It is suggesting that the exact rate of change of damping is not so critical as far as it starts low and rises with the joint angle. Consequently, the hyperbolic shape allows the spring to absorb the initial impact force without disturbance from the damper. The damping effect comes at a later stage after storing some collision energy in the spring. However, this is not the case for the other two constant damping profiles as they present a positive trend in the magnitude of the peak collision force as the value of η increases. Moreover, it can be noted that the proposed method can make the system more predictable across all values of η, Fig. 7(a). Therefore, a higher value of η (damping coefficient) can be chosen to bring the robotic joint to the desired velocity and displacement value without increasing the peak collision force and its variability.

This results in similar changes in the variability of other state variables such as post-collision peak velocity, and peak displacement due to collision. In particular, the variability of states depends on the reduction of the magnitude of the peak collision force and its variability. High variability in state transitions (post-collision peak velocity and peak displacement) push the system to failure states [7]. In addition to the improvements mentioned above, smaller variability of the post-collision peak velocity was achieved, as illustrated in Fig. 7(b). Similarly, less variability was found for peak displacement (except for η = 1.5), shown in Fig. 7(c). This confirms the effect of minimizing the peak collision force's magnitude and variability on those of other state variables.

A significant reduction of the magnitude of the peak displacement for hyperbolic angle-dependent damping profile c_h and peak damping constant c_p was observed (Fig. 4(b) and Fig. 6(b)); interestingly, their magnitudes were similar for all values of η. This means that our proposed damping profile c_h could minimise the peak displacement as much as the maximum damping profile c_p while minimising the magnitude and variability of the peak collision force and the root mean square of the power consumed by the robotic joint. This is due to the fact that both c_h and c_p provide similar high damping value at the peak displacement, which prevents the system from moving further. However, c_h only applies high damping where the angle is high and this made our control system more efficient by achieving smaller root mean square of power compared to c_m and c_p, Fig. 4(d) and Fig. 6(d). Note that this angle-dependent damping profile was implemented based on the relative robotic joint angle from the inception of a collision. This can be implemented in a control algorithm in an industrial application using force or current sensor to detect a collision to consider the relative angle. In future work, we will study the impact of such an implementation on the control strategy efficiency. In case of larger collisions causing higher angle change, the safer method is to turn the motors off (fully compliant).

Furthermore, our proposed damping profile c_h and c_p provided similar magnitudes of the post-collision peak velocity; Fig. 4(c) and Fig. 6(c). The experimental and simulation results show similar trends. The differences in exact magnitudes can come from i) Implementing high constant values of damping (c_m and c_p) at all times, especially at the time of the collision. However, in the case of hyperbolic angle-dependent damping (c_h), the damping is around its minimum value (c_0) at the time of the collision. ii) Unmodified sources of damping such as gear friction and the coefficient of restitution, can cause the difference between the experimental and simulation magnitudes. iii) the response time of the motor representing the PD controller of the robotic joint. In general, it can be noted that a high constant damping profile is not necessary to minimise the magnitude of the peak displacement and post-collision peak velocity of the robotic joint. As it was observed, high constant damping profile would minimise the magnitude of peak displacement and velocity, but it maximises their variability as well as the magnitude and variability of the peak collision force and the root mean square of the power. Our proposed hyperbolic angle-dependent damping c_h can achieve the same state reduction as the highest constant damping profile, c_p. In this study, we have also introduced a function that not only takes into account the magnitude but also the variability of peak collision force, peak post-collision velocity and displacement where the results were plotted in Fig. 8. The results confirms that our proposed hyperbolic function provides the smallest values of the Cv_r across all values of η.

TABLE IV
EXPERIMENTAL RESULTS: THE ANGLE-DEPENDENT DAMPING PROFILE VERSUS CONSTANT DAMPING PROFILES.

	Coefficient of Variation of the Robotic Joint Cv_r	
η	$\alpha\%$	$\beta\%$
0.5	-22.238	-20.740
1	-22.334	-38.426
1.5	-39.395	-35.915

There have been several studies trying to provide stability. One of the proposed methods is based on environment reaction force feedback control. However, this method raises challenges in terms of placing several sensors at the point of contact [10], [11] for the closed-loop control. Authors in [9] focused on applying a reaction force by searching policy for optimum gains for a feedback controller. Other methods involve predicting the consequence of variability on the stability of the system [12], [13]. All the methods mentioned above make the system vulnerable to external perturbations as fast collision detection, numerical calculation, control and reactive behaviour mechanisms are needed. In contrast, we propose a simple approach that can be implemented in a control algorithm or a hardware mechanism of a robotic joint without any need for sensor reading for a closed-loop control, quick reaction or sophisticated numerical calculation or control policies for predictions. This approach minimises both the magnitude and variability of collision force as well as the above stated important factors underpinning predictability and stability.

This method can be a good candidate for a multi-joint scenario because the angle-dependent damping will be implemented at a joint level. The movement of each joint due to collision will depend on the configuration of the robot

This work is licensed under a Creative Commons Attribution 4.0 License. For more information, see https://creativecommons.org/licenses/by/4.0/

This article has been accepted for publication in a future issue of this journal, but has not been fully edited. Content may change prior to final publication. Citation information: DOI 10.1109/LRA.2021.3062307, IEEE Robotics and Automation Letters

at the point of collision with an external object. The prove of stability has not been addressed in this paper. However, reasoning on the passivity of the system we can deduct that the system is stable. The proposed control algorithm is tested for a limited range of collisions. It would be interesting to test harder collisions in the future to find the range that the proposed method is useful.

IX. Conclusion

This paper, for the first time, provides experimental and analytical evidence for the ability of an angle-dependent hyperbolic damping profile in a robotic joint to reduce the peak collision force and its variability. Bio inspiration was taken from the human knee joint that is known to have an angle-dependent impedance profile. Three sets of experiments and simulations were conducted to compare the performance of the proposed hyperbolic angle-dependent damping profile with two other constant damping profiles. The results provide important design guidelines for variable impedance joints in robots to improve stability by reducing the collision force as well as its variability in closed-loop control.

Table III shows that the proposed hyperbolic angle-dependent damping profile c_h achieves peak force reduction of $\approx -22.006\%$ compared to the medium constant damping profile c_m and $\approx -26.390\%$ compared to peak constant damping profile c_p. The corresponding average variability reduction of the peak collision force was $\approx -45.922\%$ and $\approx -46.680\%$. Also, the proposed damping profile had led to a reduction of peak displacement and post-collision peak velocity, which was, at some extent, similar to when the maximum constant damping profile c_p was implemented. The proposed hyperbolic angle-dependent damping profile c_h achieved peak post-collision displacement reduction of $\approx -14.682\%$ compared to the medium constant damping profile c_m and $\approx -0.659\%$ compared to peak constant damping profile c_p. The corresponding average variability reduction of peak post-collision displacement were $\approx -35.884\%$ and $\approx -11.298\%$.

Table III also shows that the proposed hyperbolic angle-dependent damping profile c_h achieves average post-collision peak velocity reduction of $\approx -4.886\%$ compared to the medium constant damping profile c_m and $\approx -0.542\%$ compared to peak constant damping profile c_p. The corresponding average variability reduction of the post-collision peak velocity was $\approx -24.963\%$ and $\approx -39.384\%$. Furthermore, Table III shows that the proposed hyperbolic angle-dependent damping profile c_h achieves a reduction of root mean square of power up to $\approx -7.149\%$ compared to the medium constant damping profile c_m and $\approx -13.094\%$ compared to peak constant damping profile c_p.

The percentage of reduction of the coefficient of variation of the robotic joint Cv_r value as seen in Table IV of up to $\approx -27.989\%$ and $\approx -31.693\%$ was achieved when comparing the proposed hyperbolic angle-dependent damping profile c_h with medium constant damping profile c_m and the maximum constant damping profile c_p respectively. Simulation results based on a spring-variable damper-mass model has confirmed the experimental data.

References

[1] E. Ohashi, T. Aiko, T. Tsuji, H. Nishi, and K. Ohnishi, "Collision avoidance method of humanoid robot with arm force," *IEEE Transactions on Industrial Electronics*, vol. 54, no. 3, pp. 1632–1641, 2007.

[2] M. P. Polverini, A. M. Zanchettin, and P. Rocco, "Real-time collision avoidance in human-robot interaction based on kinetostatic safety field," in *2014 IEEE/RSJ International Conference on Intelligent Robots and Systems*, pp. 4136–4141, IEEE, 2014.

[3] Y. Blum, H. R. Vejdani, A. V. Birn-Jeffery, C. M. Hubicki, J. W. Hurst, and M. A. Daley, "Swing-leg trajectory of running guinea fowl suggests task-level priority of force regulation rather than disturbance rejection," *PloS one*, vol. 9, no. 6, p. e100399, 2014.

[4] J. W. Smith, J. C. Christensen, R. L. Marcus, and P. C. LaStayo, "Muscle force and movement variability before and after total knee arthroplasty: A review," *World Journal of Orthopedics*, vol. 5, no. 2, p. 69, 2014.

[5] F. Bianchi, G. Bartoli, K. Shoar, M. R. A. Fernandez, V. Pereno, J. Zirjakova, A. Jiang, and T. Nanayakkara, "Adaptive internal impedance control for stable walking on uncertain visco-elastic terrains," in *2012 IEEE/RSJ International Conference on Intelligent Robots and Systems*, pp. 2465–2470, IEEE, 2012.

[6] M. Garcia, A. Chatterjee, A. Ruina, and M. Coleman, "The simplest walking model: stability, complexity, and scaling," *J Biomech Eng*, 1998.

[7] K. Byl and R. Tedrake, "Metastable walking on stochastically rough terrain," *Proceedings of robotics: science and systems IV*, pp. 6490–6495, 2008.

[8] T. Nanayakkara, K. Byl, H. Liu, X. Song, and T. Villabona, "Dominant sources of variability in passive walking," in *2012 IEEE International Conference on Robotics and Automation*, pp. 1003–1010, IEEE, 2012.

[9] Y. Şahin, F. M. Botsalı, M. Kalyoncu, M. Tinkir, Ü. Önen, N. Yılmaz, Ö. K. Baykan, and A. Çakan, "Force feedback control of lower extremity exoskeleton assisting of load carrying human," in *Applied Mechanics and Materials*, vol. 598, pp. 546–550, Trans Tech Publ, 2014.

[10] D. Owaki, L. Morikawa, and A. Ishiguro, "Listen to body's message: Quadruped robot that fully exploits physical interaction between legs," in *2012 IEEE/RSJ International Conference on Intelligent Robots and Systems*, pp. 1950–1955, IEEE, 2012.

[11] C. D. Remy, K. Buffinton, and R. Siegwart, "Stability analysis of passive dynamic walking of quadrupeds," *The International Journal of Robotics Research*, vol. 29, no. 9, pp. 1173–1185, 2010.

[12] J. Schmitt, M. Garcia, R. Razo, P. Holmes, and R. J. Full, "Dynamics and stability of legged locomotion in the horizontal plane: a test case using insects," *Biological cybernetics*, vol. 86, no. 5, pp. 343–353, 2002.

[13] I. Wijesundera, M. N. Halgamuge, A. Nirmalathas, and T. Nanayakkara, "Predicting the mean first passage time (mfpt) to reach any state for a passive dynamic walker with steady state variability," *PloS one*, vol. 13, no. 11, p. e0207665, 2018.

[14] V. Pereno, K. Shoar, G. Bartoli, F. Bianchi, and T. Nanayakkara, "Stable walking on variable visco-elastic terrains using meta-parameters for passive state migration," in *2013 IEEE/RSJ International Conference on Intelligent Robots and Systems*, pp. 3126–3131, IEEE, 2013.

[15] N. Hogan, "Impedance control: An approach to manipulation: Part i-theory," *Journal of dynamic systems, measurement, and control*, vol. 107, no. 1, pp. 1–7, 1984.

[16] S. Masouros, A. Bull, and A. Amis, "i) biomechanics of the knee joint," *Orthopaedics and Trauma*, vol. 24, pp. 84–91, 2010.

[17] L.-Q. Zhang, G. Nuber, J. Butler, M. Bowen, and W. Z. Rymer, "In vivo human knee joint dynamic properties as functions of muscle contraction and joint position," *Journal of biomechanics*, vol. 31, no. 1, pp. 71–76, 1997.

[18] A. Radulescu, M. Howard, D. J. Braun, and S. Vijayakumar, "Exploiting variable physical damping in rapid movement tasks," in *2012 IEEE/ASME International Conference on Advanced Intelligent Mechatronics (AIM)*, pp. 141–148, IEEE, 2012.

[19] M. F. E. Morland, K. Althoefer, and T. Nanayakkara, "Novel method to form adaptive internal impedance profiles in walkers," in *2015 37th Annual International Conference of the IEEE Engineering in Medicine and Biology Society (EMBC)*, pp. 7764–7767, IEEE, 2015.

[20] M. R. Shorten and D. S. Winslow, "Spectral analysis of impact shock during running," *Journal of Applied Biomechanics*, vol. 8, no. 4, pp. 288–304, 1992.

[21] N. Hogan, "Adaptive control of mechanical impedance by co-activation of antagonist muscles," *IEEE Transactions on automatic control*, vol. 29, no. 8, pp. 681–690, 1984.

This work is licensed under a Creative Commons Attribution 4.0 License. For more information, see https://creativecommons.org/licenses/by/4.0/